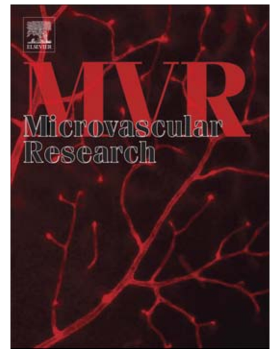

Microarterial anastomoses: A parameterised computational study examining the effect of suture position on intravascular blood flow

R.A.J. Wain, D. Hammond, M. McPhillips, W. Ahmed, J.P.M. Whitty

PII: S0026-2862(16)30009-7
DOI: doi: 10.1016/j.mvr.2016.02.003
Reference: YMVRE 3605

To appear in: *Microvascular Research*

Received date: 15 July 2015
Revised date: 4 February 2016
Accepted date: 4 February 2016

Microarterial anastomoses: a parameterised computational study examining the effect of suture position on intravascular blood flow

R. A. J. Wain

Department of Plastic & Reconstructive Surgery, University Hospital of South Manchester, Southmoor Road, Wythenshawe, Manchester, M23 9LT, UK

D. Hammond[b], M. McPhillips[a,b], W. Ahmed[b], J. P. M. Whitty[b,]*

[a]School of Postgraduate Medicine and Dentistry, University of Central Lancashire, Fylde Road, Preston, Lancashire PR1 2HE, UK
[b]School of Computing, Engineering and Physical Sciences, University of Central Lancashire, Fylde Road, Preston, Lancashire, PR1 2HE, UK

Abstract

This study investigates the extent to which individual aspects of suture placement influence local haemodynamics within microarterial anastomoses. An attempt to physically quantify flow characteristics of blood past microvascular sutures is made using Computational Fluid Dynamics (CFD) software. Particular focus has been placed on increased shear strain rate (SSR), a known precipitant of intravascular platelet activation and thrombosis.

Measurements were taken from micrographs of sutured anastomoses in chicken femoral vessels, with each assessed for bite width, suture angle and suture spacing. Computational geometries were then created to represent the anastomosis. Each suture characteristic was parameterised to allow independent or simultaneous adjustment. Flow rates were obtained from anonymised Doppler ultrasound scans of analogous vessels during preoperative assessment for autologous breast reconstruction. Vessel simulations were performed in 2.5mm ducts with blood as the working fluid. Vessel walls were non-compliant and a continuous Newtonian flow was applied, in accordance with current literature.

*Corresponding author
Email address: `jwhitty@uclan.ac.uk` (J. P. M. Whitty)

Suture bite angle and spacing had significant effects on local haemodynamics, causing notably higher local SSRs, when simulated at extremes of surgical practice. A combined simulation, encompassing subtle changes of each suture parameter simultaneously i.e. representing optimum technique, created a more favourable SSR profile. As such, haemodynamic changes associated with optimum suture placement are unlikely to influence thrombus formation significantly. These findings support adherence to the basic principles of good microsurgical practice.

Keywords: Microvascular; Microarterial; Anastomosis; Suture; Parameterised; Computational Fluid Dynamics (CFD); Computational modelling; Blood flow.

1. Introduction

The first successful end-to-end anastomosis was reported by Jassinowski [1] in 1889 using fine silk sutures to coapt sheep carotid arteries. Shortly after, in 1912, Alexis Carrel was awarded the Noble Prize for Physiology and Medicine for his work on the triangulation method of placing vascular sutures [2]. Microvascular anastomosis was the natural progression of this pioneering work, and was first performed in laboratory animal vessels as small as 1.4mm diameter by Jacobson in 1960 [3]. This paved the way for the advances in microsurgery seen in the last 50 years including replantation of limbs and digits, transplantation surgery and routine use of free-tissue transfer for reconstructive procedures.

Many techniques have been described for performing microvascular anastomoses, and these are broadly classified into *suture* and *non-suture* methods. Although simple interrupted sutures are widely regarded as the standard technique, several other sutured methods have been described including continuous, locking, and mattress amongst others. A systematic review of the literature concluded there was no statistical difference in short- and/or long-term patency rates between the various sutured techniques, provided standard microsurgical principles were adhered to, including eversion of the suture line, minimal tension, and intima-to-intima contact [4]. Non-suture methods of anastomosis are varied and numerous and include clips/staples [5, 6], glue [7], dissolving gels [8], laser [9] and the more widely used venous ring-pin coupling device [10].

Computational Fluid Dynamics (CFD)[1] is a method by which complex fluid flows can be simulated using sophisticated mathematical algorithms in order to better understand flow patterns in environments which would be impossible to demonstrate such experimentally. This technology has developed rapidly since the pioneering work of Perktold [11] and has been used to investigate local blood flow patterns for a wide range of vascular applications [12, 13]. There has however, been little work investigating microvascular surgical procedures, in particular microanastomoses, using CFD. Studies carried out by Al-Sukhun *et al.* [14] and Rickard *et al.* [15] have explored this area but have not specifically addressed the effects of suture placement on local haemodynamics. Previous work carried out by our group has accounted for suture geometry, however these were very much idealised simulations [16]. We were unable to identify any previous parameterised studies in the existing literature investigating anastomotic flows or suture position.

Whilst intravascular stasis undoubtedly contributes to thrombus formation [17], Shear Strain Rate (SSR), defined as the rate of change of strain when a shear stress is applied, is more reliable than flow-rate or velocity when evaluating coagulation within flow [18]. This is because surface transport phenomena

[1] *Abbreviations*

ANOVA - Analysis of Variance

CAD - Computer Aided Design

CATIA - Computer Aided Three-Dimensional Interactive Application

CFD - Computational Fluid Dynamics

CI - Confidence Interval

DIEA - Deep Inferior Epigastric Artery

Fisher's LSD - Fisher's Least Significant Difference

FSI - Fluid Structure Interaction

SSR - Shear Strain Rate

WSS - Wall Shear Stress

PSV - Peak Systolic Velocity

govern the SSR and demonstrates the velocity change as distance from the wall increases [19]. SSR is proportional to Wall Shear Stress (WSS), which is the tangential force of flowing blood on the vessel endothelium, and is a known contributor to formation of atherosclerosis [20, 21, 22, 23]. Both high WSS and SSR are known to activate platelets within flowing blood [17, 24, 25, 26, 27], which is critical when investigating intravascular thrombosis, as activated platelets become adherent, forming aggregates and subsequently thrombus. To compound these effects, shear-induced platelet thrombus formation activates coagulation factors which in turn promotes further fibrin generation [28]. Excessive generation of fibrin is itself a direct precipitant of thrombosis. Platelets activated by high shear elicit procoagulant activity [29] and also bind preferentially to exposed subendothelium and injured vascular endothelium [18], although do not have the same affinity for pristine vessel walls [30].

It is difficult to put an absolute value on the point at which thrombosis is initiated, however SSRs of greater than around 1000s^{-1} have been shown to cause direct platelet activation in studies by Roth [26] and Shen [25]. In addition, a positive relationship was identified between SSR and thrombus accumulation rates at high SSRs, with thrombus growth rates being up to four times greater in high SSR simulations i.e. up to 6000s^{-1}, than for physiological shear rates of less than 400s^{-1}[31].

1.1. Scope of study

The present study represents an evolution from previous work comparing flow characteristics in idealised sutured and coupled microvascular anastomoses [16]. The parameterised geometries used here more closely resemble clinical practice and will examine blood flow properties through microarterial sutured anastomoses, specifically with the aim of evaluating the effect of suture placement and position on intravascular flow.

2. Materials and methods

A range of factors were taken into consideration when designing this study in an attempt to create realistic geometries for the computational simulations. Each of these will be discussed in detail and creation of the computational models subsequently described.

2.1. Suture characteristics

A series of microarterial anastomoses, consisting of 45 individual sutures, was performed on chicken femoral arteries under an operating microscope using 9/0 Ethilon (Ethicon, Johnson & Johnson, Somerville, NJ 08876, USA) microsuture. Each anastomosis was performed end-to-end using a standard interrupted suture technique and microsurgical instruments. A strip of 1mm microgrid background material was placed behind each anastomosis to provide a consistent objective scale for subsequent imaging. This model was chosen as the chicken femoral artery closely represents the Deep Inferior Epigastric Artery (DIEA) which is commonly anastomosed during breast reconstructive surgery using free-tissue transfer. The intralumenal surface of each anastomosis was then exposed and a micrograph image produced, Figure 1, to analyse suture placement properties including: number of sutures, size of bite, distance between sutures and angle of bite. Measurements of each of these characteristics was made by analysing micrographs using the Computer Aided Three-Dimensional Interactive Application (CATIA) Computer Aided Design (CAD) code, as shown in Figure 2. The variation of each parameter was analysed, with the upper and lower limits at the 95% confidence interval (CI) calculated. F

2.2. Vessel flow rates

Blood flow was measured in 10 DIEAs using Doppler ultrasonography as part of pre-operative assessment for free-tissue transfer breast reconstruction. A Phillips iU22 ultrasound scanner and L9-3 probe (Philips Healthcare, 5680 DA Best, The Netherlands) was used to obtain these values. Vessel diameter and Peak Systolic Velocity (PSV) were recorded for each DIEA and calculated

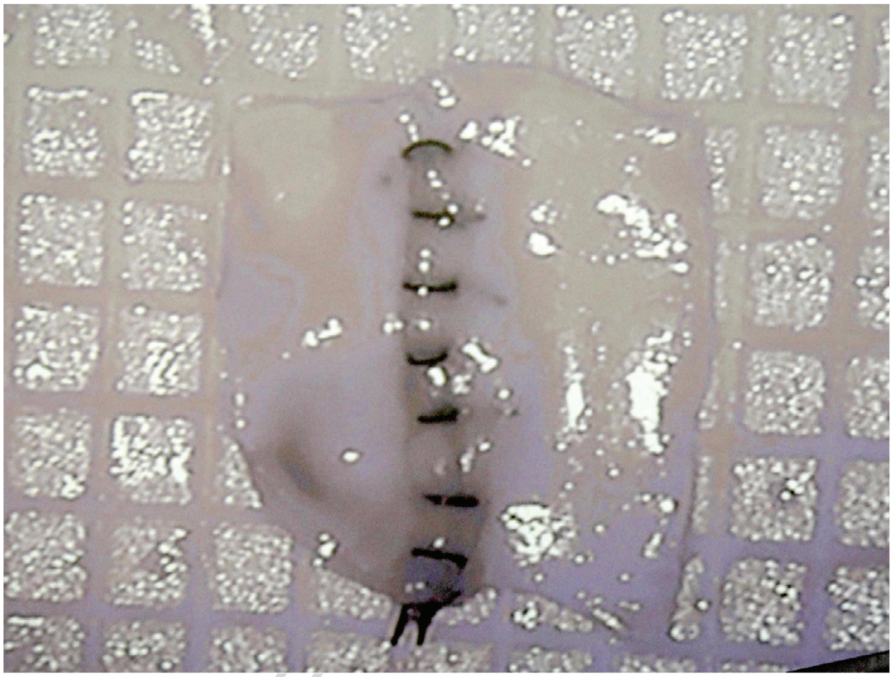

Figure 1: Micrograph of chicken femoral arterial anastomosis demonstrating suture positioning (*1mm microgrid background*)

means of these values were used as inlet properties for the vascular simulations. Only raw data specifically pertaining to vessel characteristics and flow rates were provided for this purpose with all patient-identifiable details withheld.

2.3. Computational model

Specific steps taken to produce the computational simulations are presented individually including creation of the vessel geometry and application of the appropriate boundary conditions. Post simulation analysis methods are also given herein.

2.3.1. Geometry creation and meshing

The sutured anastomosis geometry was created using the Design-Modeler module within ANSYS Workbench v14.5 simulation code. A vessel of diameter 2.5mm and length 10mm was formed, and a series of 8 suture bites of

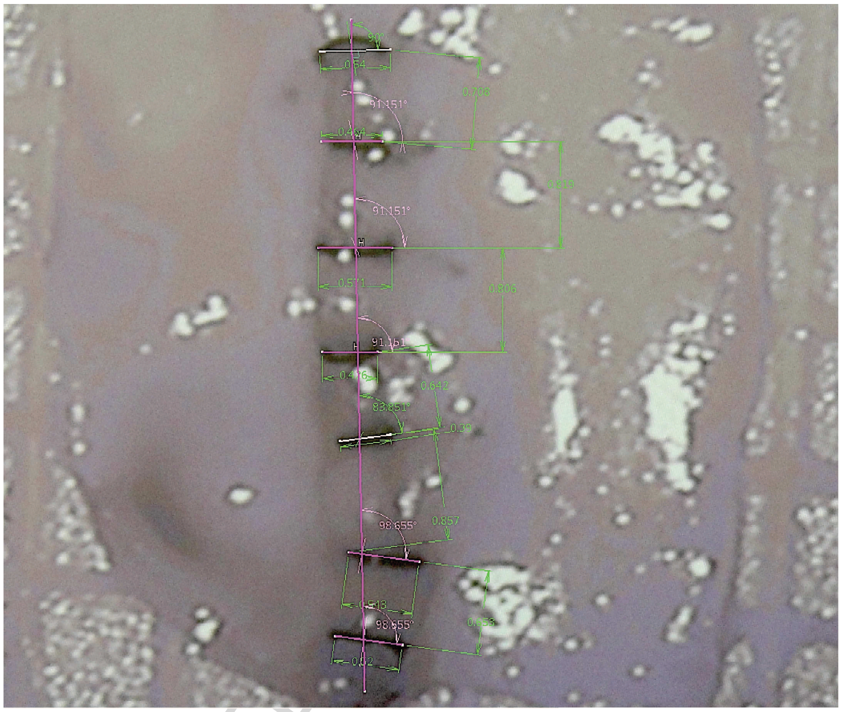

Figure 2: Measurement of suture parameters using CATIA (*lengths (mm), angles (degrees)*)

0.04mm diameter material (simulating 9/0 Ethilon microvascular suture) were placed circumferentially around the central portion of the vessel to resemble the anastomotic site. Each suture bite consisted of a cylindrical longitudinal portion, with curved leading and trailing edges, set partially into the vessel wall to account for the deformation of the intimal surface. The bite width, orientation, and spacing of each suture being parameterised such that each could be individually adjusted within the limits set by statistical analysis of the measured micrographs. Geometries were modified to include a portion of the vessel representing just less than half of the volume and surface with an appropriate symmetry condition applied in the longitudinal axis, see §§§2.3.2. This permitted excellent visualisation of the internal flows in post-processing and reduced computational expense and simulation time. In addition, analysis of this vascular section also allowed demonstration of a range of suture configurations on a single simulation. Meshes for each geometry were subsequently created within ANSYS Meshing v14.5 using tetrahedral cells.

2.3.2. Boundary conditions

In keeping with current literature [11, 32, 33, 34], blood was modelled as a Newtonian fluid with a density of 1060kgm^{-3}, viscosity of 3.5μPas, and in a steady-state. The vessel wall was non-compliant with no-slip conditions and was simulated using a laminar solver due to the low Reynolds number (Re ~500). Despite opinions within the literature regarding the need for non-Newtonian solvers when simulating blood flow [35], we have demonstrated, using the non-Newtonian Carreau-Yasuda model, that results are universally unaffected by this in our geometries (§§3.5). As such, we have continued to use a Newtonian model for simplicity. Both inlet and outlet velocities were set to 70cms^{-1}, as calculated from the mean DIEA PSV provided by preoperative Doppler ultrasound scans. A paraboloid inlet configuration was applied to ensure fully developed flow prior to the anastomosis. As mentioned in Geometry creation and shown in Figure 3, a symmetry boundary condition was applied to the internal surfaces.

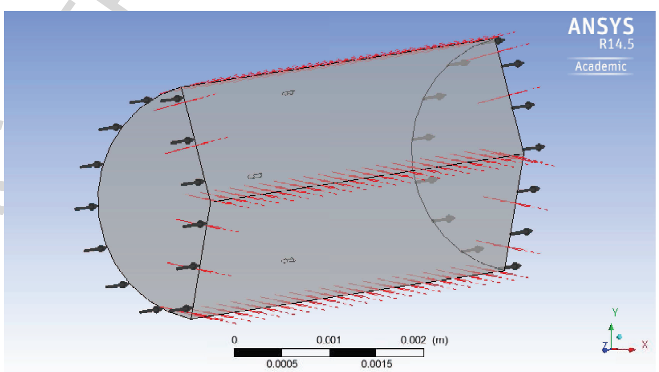

Figure 3: Vessel geometry - Demonstrating three sutures within the wall, blood flow direction (*black arrows*), and symmetry (*red arrows*)

2.3.3. Simulation and post-processing

Three simulations were carried out investigating the influence of each suture parameter i.e. bite width, spacing and angle on intravascular flow properties.

Individual simulations contained three sutures, each with a statistical maximum, mean, or minimum value calculated at the 95% CI from the micrographic measurements. A fourth simulation was performed encompassing a smaller degree of change in all of the parameters to more closely resemble clinical practice, with a final simulation using the non-Newtonian Carreau-Yasuda model to investigate its significance in our geometries

Blood is well known to be a non-Newtonian fluid [36] meaning that the shear stress at any point in the fluid is not proportional to the velocity gradient or, in the case of a fluid undergoing pure shear, the strain rate. Due to chemical and physiological phenomena, at low strain rates [37] and in very small diameter vessels (20-500μm) [38], blood may exhibit non-Newtonian shear-thinning behaviour.

The ANSYS-CFX software used to perform the computational modelling calculations in this work has seven non-Newtonian models at its disposal, of particular interest to shear-thinning blood rheology is the Carreau-Yasuda model. In the non-Newtionian simulations conducted in this work the Carreau-Yasuda was employed:

$$\mu = \mu_\infty + \frac{\mu_o - \mu_\infty}{\{1 + (\lambda\dot{\gamma})^a\}^{\frac{1-n}{a}}} \tag{1}$$

where μ_o is the low shear viscosity, μ_∞ is the high shear viscosity, λ is the time constant and a is the Yasuda exponent. The advantage of this model is that the transitions from non-Newtonian to Newtonian behaviour, at both high and low shear rates, are adequately described. Additionally, as evident in the literature [39, 40, 41, 35, 42, 43], this particular model is favoured when simulating non-Newtonian blood flows.

In keeping with our previous work on this subject [16], we elected to create near-wall (boundary layer) velocity profiles to visualise flow in the region of the anastomosis, as well as pressure, WSS and SSR profiles to gain an appreciation of potential for platelet activation and thus thrombosis.

3. Results

The results of each simulation are presented in turn, with specific focus on the SSR. As WSS is directly proportional to SSR, values for both are not presented separately as any change in one is reciprocated in the other. With respect to velocity and pressure, the overall profiles remain consistently unchanged throughout the portion of vessel simulated in all geometries. There are, as would be expected, slight alterations in boundary layer (near-wall) velocity at the sutures themselves (Figure 4), although the magnitude is not significant. Throughout this section simulations comprising three variable groups i.e. bite width, angle and the combined geometry, have been subjected to statistical analysis using the analysis of variance (ANOVA) technique, with those having two variable groups i.e. suture spacing, undergoing the Student's t-test. Mean and maximum SSR values were obtained from the vessel wall in the immediate vicinity of each suture via a defined 'user surface' function within ANSYS CFX Post software.

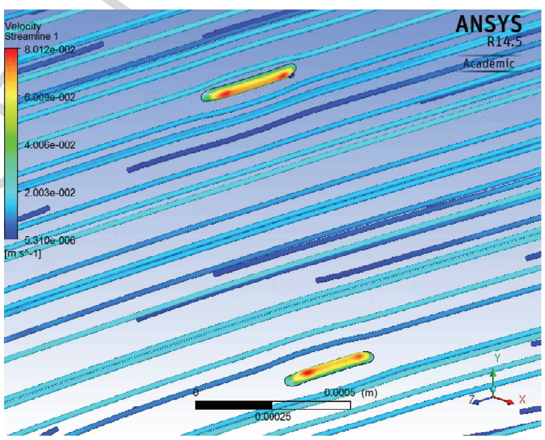

Figure 4: Near-wall (boundary) velocity streamlines at the anastomosis

3.1. Suture bite width

Three different bite widths were evaluated, these were small (0.35mm), intermediate (0.385mm) and large (0.42mm) as calculated from measured suture bites on the micrographed anastomoses. In these simulations bite width was the only variable considered, with suture spacing and angle remaining constant. The SSR distribution is shown in Figure 5, which demonstrates an increase in SSR around each suture, although this does not appear to be specifically related to the size of suture bite. Mean SSRs for small, intermediate and large bites were 1196s^{-1}, 1194s^{-1}, and 1167s^{-1} respectively. Statistical analysis using the ANOVA tool confirmed this observation.

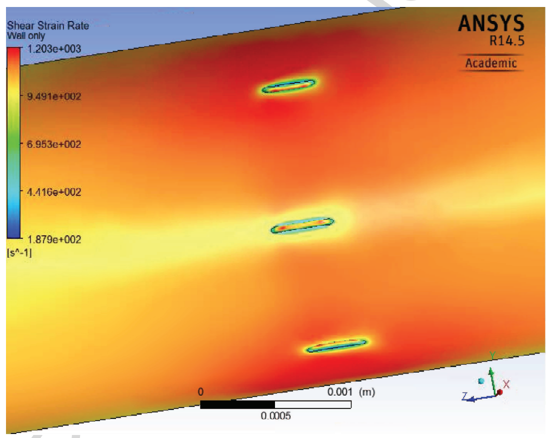

Figure 5: SSR distribution at suture sites after variation in bite width

3.2. Suture bite angle

Again, three sutures were simulated to investigate the effect of angle on local haemodynamics, with their values being set to minimum (-20^o), average (0^o) and maximum (20^o). This angle represents deviation from the *standard* suture perpendicular to the line of the anastomosis and was the only variable changed in this simulation. Areas of higher SSR are found surrounding the sutures with greater deviation from 0^o, either in the positive or negative direction, as demonstrated in Figure 6. Mean SSR for angled sutures is 1195s^{-1} and 1191s^{-1} for 20^o and -20^o respectively, with the mean for 0^o being 1128s^{-1}. Statistical evaluation using ANOVA revealed a highly significant difference between the SSRs of different bite angles in this group.

These mean values can be verified by comparing with those obtained from a cogent analytical model for rigid pipe flow (*Poiseuille*), the ratio of shear stress ($\tau(r)$) to viscosity, thus [44]:

$$\dot{\gamma(r)} = \frac{\tau(r)}{\mu} = \frac{4\dot{m}}{\pi\rho r^3} = \frac{4\dot{Q}}{\pi r^3} \qquad (2)$$

where, $\dot{m} = \rho\pi R^2 u(z)$, is the mass flow-rate, ρ is the blood density (1060 kgm^{-3}) and spacial coordinate r (radius) is the distance from the centre to the shear layer of blood within the vessel; additionally $\dot{Q}$ represents the volumetric flow rate. Direct application of equation (2) with the spacial coordinate set to the inner (lumenal) radius of the vessel gives $\gamma(R_i) = 1120\,\mathrm{s}^{-1}$ which compares favourably with the value of $1115 \pm 39\,\mathrm{s}^{-1}$ for a pristine vessel (at the 95% confidence level).

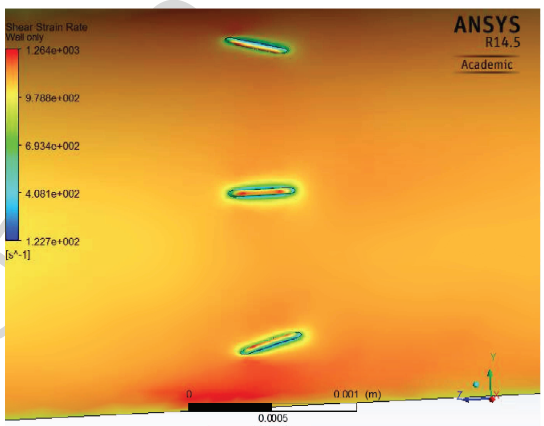

Figure 6: SSR distribution at suture sites after variation in bite angle

3.3. Suture spacing

Distances between three sutures were modelled giving two parameters labelled as wide (0.82mm) and narrow (0.48mm). All sutures had identical bite widths and were orientated perpendicularly to the anastomosis. High concentrations of SSR were found in the areas surrounding the sutures with a particular focus in the region between the closely placed sutures (mean SSR $1168\mathrm{s}^{-1}$) compared to the wider gap (mean SSR $1101\mathrm{s}^{-1}$) as shown in Figure 7. Statistical evaluation using the Student's t-test revealed a highly significant difference in this group.

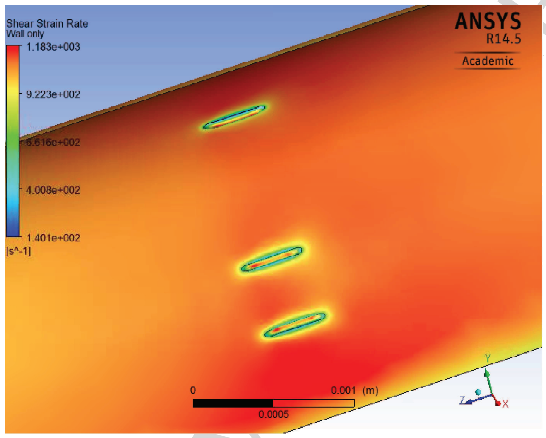

Figure 7: SSR distribution at suture sites after variation in suture spacing

3.4. Combined suture parameters

This simulation also consisted of three sutures, again with the same overall geometry, however each suture had been parameterised to minor variations in each of bite width, angle and spacing simultaneously in order to most accurately represent a realistic microsurgical anastomosis. The variation has been kept within the extremes of practice i.e. within one standard deviation of the mean for each parameter. Top, middle and bottom sutures had bite widths of 0.35mm, 0.42mm, and 0.39mm, and angles of -10^o, 10^o, and -5^o respectively. Suture spacing was 0.6mm between top and middle, and 0.7mm between middle and bottom sutures. This simulation demonstrates areas of higher SSR in the vicinity of the sutures (Figure 8) although there was no statistical significance between individual sutures.

3.5. Newtonian vs. non-Newtonian simulation

Analogous geometries were formed to explore the influence of blood as a non-Newtonian fluid on our simulations. Two identical geometries were given

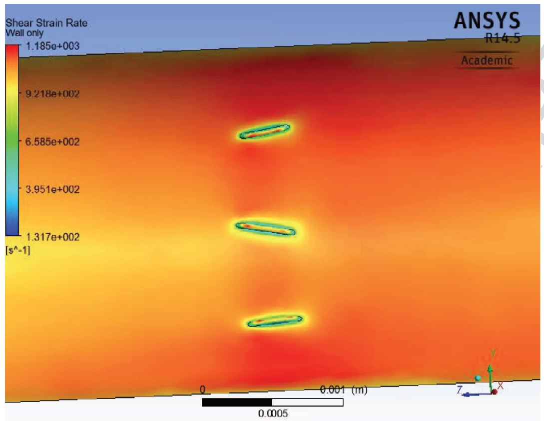

Figure 8: SSR distribution at suture sites after variation in all parameters

identical boundary conditions with the exception of their viscous fluid properties. As for the previous simulations, there was no discernible difference in any of the primary parameters i.e. velocity or pressure fields. Whilst the same picture of elevated SSR is seen surrounding the sutures (Figure 9) the difference between Newtonian and non-Newtonian solutions is negligible. Mean SSR readings at identical points in the simulations were $1106s^{-1}$ and $1104s^{-1}$ for Newtonian and non-Newtonian fluids respectively, demonstrating no statistical significance between the groups using the Student's t-test.

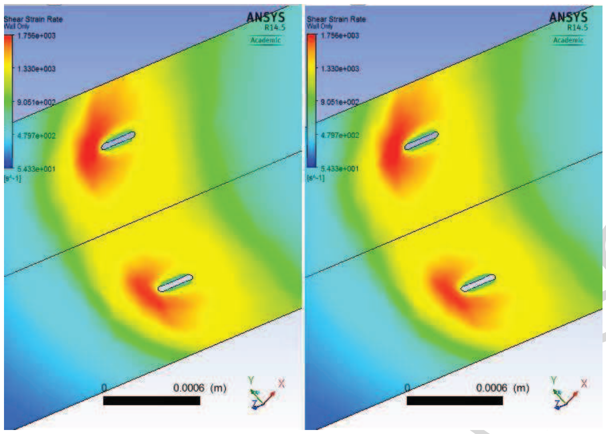

Figure 9: SSR distribution at suture sites in comparative Newtonian (*left*) and non-Newtonian (*right*) simulations

4. Discussion

The aim of this study was to investigate the extent to which individual aspects of suture placement influence local haemodynamics within microarterial anastomoses. A parameterised computational simulation has been created with realistic geometries in an attempt to address this question, as to do so *in vivo* would present tremendous difficulty.

The interrupted suture method is largely regarded as standard practice, although microsurgical suture techniques vary widely. It has been found clinically that provided sound microsurgical principles were adhered to, patency rates of these alternative methods do not differ significantly [4]. For this reason, we feel it acceptable to use the conventional interrupted technique as a basis for the suture geometry creation. Available literature examining microvascular anastomotic flow is limited, confined to a few computational studies [14, 15, 45], with the effect of suture placement on intravascular flow being negated. Previous work by our group has taken into consideration sutures at the anastomotic site [16], although these were idealised geometries. There have been more recent attempts at imaging anastomotic flow intraoperatively to more closely examine their characteristics [46] however, despite this excellent technology, the anastomosis can not be visualised in sufficient detail to evaluate the impact of suture placement on flow.

4.1. Key findings

The present study has individually parameterised each key variable within the suture technique, namely bite width, bite angle, and suture spacing to establish any influence on flow. Of these factors, suture bite angle and suture spacing had significant effects on the local haemodynamics, causing notably higher SSRs in these regions. At the maximum and minimum limits (20^o and -20^o) of suture angle variation, SSRs had significantly increased from those in ideal perpendicular placement (0^o). These findings were confirmed statistically using an ANOVA (Table 1) at the 5% confidence level (p-value 0.00004) followed by Fisher's LSD post-hoc test. Interpretation of this link between bite angle and high SSR implies that at the extremes of practice there may be a increased risk of platelet activation and hence thrombus formation. Whilst there are no previous studies with which to directly compare our results, this finding is in keeping with conventional teaching of microsurgical principles and practice [47, 48] i.e. to ensure sutures are placed perpendicular to the anastomosis.

Source of Variation	SS	df	MS	F	$p-level$	$F-critical$
Between groups	14269	2	7134	26.45	0.00004	3.89
Within groups	3237	12	269	-	-	-
Total	17506	14				

Table 1: ANOVA table for suture angle SSR

Similar reasoning can be given for the findings related to suture spacing, where literature is sparse. In our simulations we demonstrated a statistically significant increase in SSR when spacing between sutures was narrow compared to wide. Data were analysed using a Student's t-test (Table 2) at the 5% confidence level (p-value 0.00002). We can therefore surmise that sutures placed closely to one another produce high SSRs, which has the potential to activate

Degrees of freedom	8	Hypothesized Mean Difference	0
Test statistics ($t - value$)	8.19	Pooled Variance	165.4
One-tailed distribution			
$p - level$	0.00002	$t - critical(5\%)$	1.86

Table 2: Student's t-test table for suture spacing SSR

platelets and promote blood clotting. Simulations were again performed at the extremes of surgical practice and, whilst these data would imply that large gaps should be left between sutures, of course this must be balanced with the need for a well-sealed anastomosis.

Interestingly, suture bite width alone did not produce a significant difference in anastomotic SSRs, even at the extremes of practice. In fact, SSR distributions around sutures of varied bite width were almost identical. Conventional teaching advocates evenly placed bites either side of the anastomosis approximately 1.5 times the thickness of the wall from the open vessel end [47, 48], permitting sufficient tissue to grasp whilst preventing bunching. Our results neither support nor reject current practice, as we have not considered the elastic properties of the vessel wall and hence not investigated the potential impact of vessel bunching. It would therefore be reasonable to state that bite width does not independently influence local haemodynamics in these simulations, but is likely to be significant both in clinical practice and in future simulations when addressing vascular wall compliance.

Although suture bite angle and suture spacing produced statistically significant differences in their results, the findings of our combined simulations were also notable. Sutures were parameterised to produce smaller, more clinically realistic changes in all aspects i.e. avoiding the extremes of practice. Lower overall mean SSRs were identified in these models ($\sim 1130 \mathrm{s}^{-1}$) compared to those found at the limits of normal practice in the individual parameter models $\sim 1195 \mathrm{s}^{-1}$ for angle, and $\sim 1170 \mathrm{s}^{-1}$ for spacing. SSRs were largely similar in the vicinity of each suture in the combined simulation, indicating that subtle variances in suture placement are unlikely to influence thrombus formation. Whether the lower SSR in the combined simulation would reflect a significant reduction in thrombus formation is difficult to predict from the available data. What can be stated is that as SSR increases, platelet activation occurs and thrombus growth rates increase [26, 31], hence a technique that may improve the local haemodynamics and thereby reduce SSR, should be adopted.

In addition, in an attempt to ensure the symmetry boundary condition did not influence results, a whole vessel was also constructed and simulated, see Figure 10. This produced mean SSRs of comparable magnitude and distribution to those in the symmetry boundary condition, thereby demonstrating appropriate use of the symmetry boundary.

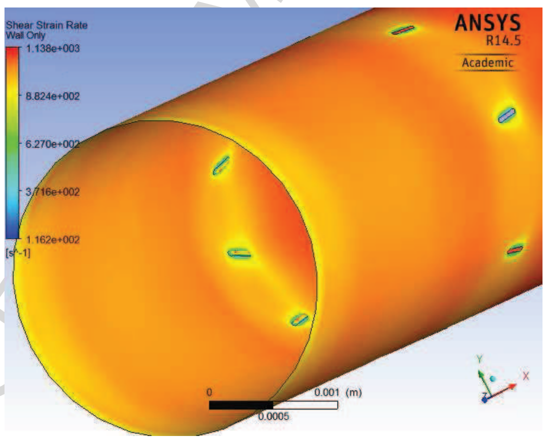

Figure 10: SSR distribution in a whole vessel geometry

Comparison of our simulations using both Newtonian and non-Newtonian fluid solvers revealed almost identical values for each of the baseline outputs i.e velocity and pressure profiles, as well as project specific outputs including WSS and SSR. We can therefore conclude that the Newtonian assumption is appropriate in the simulations performed here (§§3.5).

4.2. Limitations

Although great care has been taken to ensure that geometries created herein represent clinical practice as closely as possible, several assumptions have been made regarding the boundary conditions which do not transfer directly to an *in vivo* context. The key assumptions made here are steady-state blood flow and non-compliant vessel walls, in keeping with previous studies [11, 32, 33, 34, 15, 16]. Although these conditions are not seen in real blood vessels, they permit evaluation of important flow properties pertinent to thrombosis formation, amongst others. The addition of pulsatile blood flow and vessel wall compliance to these simplified, yet robust, simulations will be addressed in our subsequent work.

5. Conclusions

Several conclusions can be drawn from these computational simulations, with both suture angle and suture spacing independently affecting anastomotic SSR.

- Greater suture angles cause greater SSRs; and as suture angles approach zero i.e. more perpendicular to the anastomosis, SSRs are kept to a minimum.
- Close suture spacing increases SSR; and wider suture spacing minimises SSRs, although balance needs to be obtained to maintain a well-sealed anastomosis.
- Small variance in all parameters i.e. optimum surgical practice, does not significantly influence flow properties in these steady-state, non-compliant models.

Our computational medical mechanics group are currently exploring the natural progression of these models i.e. pulsatile flow, incorporating vessel wall compliance, and fluid-structural interactions (FSI), with the aim of providing more realistic microvascular flow simulation.

Conflict of interest

The authors declare there are no actual or potential conflicts of interest.

355 *Acknowledgements*

The authors would like to thank the Vascular Studies Unit at the University Hospital of South Manchester NHS Foundation Trust, for providing anonymised vascular data for creation of inlet profiles and geometries. In addition, we would like to thank Mr S Iyer and Mr J R Srinivasan, Consultant Plastic Surgeons at Lancashire Teaching Hospitals NHS Foundation Trust, for their assistance in performing microvascular anastomoses for analysis.

References

[1] A. Jassinowski, Die Arteriennhat: Eine experimentelle Studie, Inaug Diss Dorpat (1889) 1–103.

[2] A. Carrel, La technique operatoire des anastomoses vasculaires et la transplantation des visceres, Lyon med 98 (1902) 859–864.

[3] Jacobson JH II, Suarez EL, Microsurgery in anastomosis of small vessels, Surg Forum 11 (1960) 243–5.

[4] M. S. Alghoul, C. R. Gordon, R. Yetman, G. M. Buncke, M. Siemionow, A. M. Afifi, W. K. Moon, From simple interrupted to complex spiral: a systematic review of various suture techniques for microvascular anastomoses, Microsurgery 31 (1) (2011) 72–80. doi:10.1002/micr.20813.

[5] C. Reddy, D. Pennington, H. Stern, Microvascular anastomosis using the vascular closure device in free flap reconstructive surgery: A 13-yea Journal of Plastic, Reconstructive & Aesthetic Surgery: JPRAS 65 (2) (2012) 195–200. doi:10.1016/j.bjps.2011.08.041.
URL http://www.ncbi.nlm.nih.gov/pubmed/21992937

[6] J. L. Maher, K. R. Roehl, R. C. Mahabir, A prospective evaluation of U-clips for arterial microvascular anastomoses, Journal of Reconstructive Microsurgery 28 (8) (2012) 543–548. doi:10.1055/s-0032-1315775.

[7] C. V. Bowen, D. H. Leach, N. L. Crosby, R. Reynolds, Microvascular anastomoses. A comparative study of fibrinogen adhesive and interrupted suture techniques, Plastic and Reconstructive Surgery 97 (4) (1996) 792–800.

[8] E. I. Chang, M. G. Galvez, J. P. Glotzbach, C. D. Hamou, S. El-ftesi, C. T. Rappleye, K.-M. Sommer, J. Rajadas, O. J. Abilez, G. G. Fuller, M. T. Longaker, G. C. Gurtner, Vascular anastomosis using controlled

phase transitions in poloxamer gels, Nature Medicine 17 (9) (2011) 1147–1152. doi:10.1038/nm.2424.

[9] A. F. Flemming, M. J. Colles, R. Guillianotti, M. D. Brough, S. G. Bown, Laser assisted microvascular anastomosis of arteries and veins: laser tissue welding, British Journal of Plastic Surgery 41 (4) (1988) 378–388.

[10] L. T. Ostrup, A. Berggren, The UNILINK instrument system for fast and safe microvascular anastomosis, Annals of Plastic Surgery 17 (6) (1986) 521–525.
URL http://www.ncbi.nlm.nih.gov/pubmed/3827122

[11] K. Perktold, H. Florian, D. Hilbert, Analysis of pulsatile blood flow: a carotid siphon model, Journal of Biomedical Engineering 9 (1) (1987) 46–53.
URL http://www.ncbi.nlm.nih.gov/pubmed/3795904

[12] F. Migliavacca, G. Dubini, Computational modeling of vascular anastomoses, Biomechanics and Modeling in Mechanobiology 3 (4) (2005) 235–250. doi:10.1007/s10237-005-0070-2.
URL http://www.ncbi.nlm.nih.gov/pubmed/15772842

[13] C. A. Taylor, D. A. Steinman, Image-based modeling of blood flow and vessel wall dynamics: applications Annals of Biomedical Engineering 38 (3) (2010) 1188–1203. doi:10.1007/s10439-010-9901-0.
URL http://www.ncbi.nlm.nih.gov/pubmed/20087775

[14] J. Al-Sukhun, C. Lindqvist, N. Ashammakhi, H. Penttilä, Microvascular stress analysis. Part I: simulation of microvascular anastomoses using finite element analys The British Journal of Oral & Maxillofacial Surgery 45 (2) (2007) 130–137. doi:10.1016/j.bjoms.2005.11.022.
URL http://www.ncbi.nlm.nih.gov/pubmed/16458394

[15] R. F. Rickard, C. Meyer, D. A. Hudson, Computational modeling of microarterial anastomoses with size discrepancy (small-to-large), The Journal of Surgical Research 153 (1) (2009) 1–11.

doi:10.1016/j.jss.2008.02.038.
URL http://www.ncbi.nlm.nih.gov/pubmed/18849053

[16] R. A. J. Wain, J. P. M. Whitty, M. D. Dalal, M. C. Holmes, W. Ahmed, Blood flow through sutured and coupled microvascular anastomoses: a comparative computational study, Journal of plastic, reconstructive & aesthetic surgery: JPRAS 67 (7) (2014) 951–959. doi:10.1016/j.bjps.2014.03.016.

[17] G. D. O. Lowe, Virchow's triad revisited: abnormal flow, Pathophysiology of haemostasis and thrombosis 33 (5-6) (2003) 455–457. doi:10.1159/000083845.
URL http://www.ncbi.nlm.nih.gov/pubmed/15692260

[18] K. S. Sakariassen, P. F. Nievelstein, B. S. Coller, J. J. Sixma, The role of platelet membrane glycoproteins Ib and IIb-IIIa in platelet adherence to human artery suben
British journal of haematology 63 (4) (1986) 681–691.
URL http://www.ncbi.nlm.nih.gov/pubmed/2942171

[19] R. F. Ismagilov, A. D. Stroock, P. J. A. Kenis, G. Whitesides, H. A. Stone, Experimental and theoretical scaling laws for transverse diffusive broadening in two-phase laminar flows
Applied Physics Letters 76 (17) (2000) 2376–2378. doi:doi:10.1063/1.126351.
URL http://apl.aip.org/resource/1/applab/v76/i17/p2376_s1?isAuthorized=no

[20] D. N. Ku, D. P. Giddens, C. K. Zarins, S. Glagov, Pulsatile flow and atherosclerosis in the human carotid bifurcation. Positive correlation between plaque l
Arteriosclerosis (Dallas, Tex.) 5 (3) (1985) 293–302.
URL http://www.ncbi.nlm.nih.gov/pubmed/3994585

[21] N. DePaola, M. A. Gimbrone, Jr, P. F. Davies, C. F. Dewey, Jr, Vascular endothelium responds to fluid shear stress gradients, Arteriosclerosis and Thrombosis: A Journal of Vascular Biology / American Heart Association 12 (11) (1992) 1254–1257.
URL http://www.ncbi.nlm.nih.gov/pubmed/1420084

[22] A. M. Shaaban, A. J. Duerinckx, Wall shear stress and early atherosclerosis: a review, AJR. American journal of roentgenology 174 (6) (2000) 1657–1665. URL http://www.ncbi.nlm.nih.gov/pubmed/10845502

[23] C. G. Caro, N. J. Cheshire, N. Watkins, Preliminary comparative study of small amplitude helical and conventional ePTFE arteriovenous shunts Journal of the Royal Society, Interface / the Royal Society 2 (3) (2005) 261–266. doi:10.1098/rsif.2005.0044. URL http://www.ncbi.nlm.nih.gov/pubmed/16849184

[24] J. J. Hathcock, Flow effects on coagulation and thrombosis, Arteriosclerosis, thrombosis, and vascular biology 26 (8) (2006) 1729–1737. doi:10.1161/01.ATV.0000229658.76797.30. URL http://www.ncbi.nlm.nih.gov/pubmed/16741150

[25] F. Shen, C. J. Kastrup, Y. Liu, R. F. Ismagilov, Threshold response of initiation of blood coagulation by tissue factor in patterned microfluidic capillaries Arteriosclerosis, thrombosis, and vascular biology 28 (11) (2008) 2035–2041. doi:10.1161/ATVBAHA.108.173930. URL http://www.ncbi.nlm.nih.gov/pubmed/18703776

[26] G. J. Roth, Developing relationships: arterial platelet adhesion, glycoprotein Ib, and leucine-rich glycopro Blood 77 (1) (1991) 5–19. URL http://www.ncbi.nlm.nih.gov/pubmed/1984803

[27] M. H. Kroll, J. D. Hellums, L. V. McIntire, A. I. Schafer, J. L. Moake, Platelets and shear stress, Blood 88 (5) (1996) 1525–1541. URL http://www.ncbi.nlm.nih.gov/pubmed/8781407

[28] H. J. Weiss, V. T. Turitto, H. R. Baumgartner, Role of shear rate and platelets in promoting fibrin formation on rabbit subendothelium. Studies utilizing The Journal of clinical investigation 78 (4) (1986) 1072–1082. doi:10.1172/JCI112663. URL http://www.ncbi.nlm.nih.gov/pubmed/3760183

[29] J. Jesty, W. Yin, P. Perrotta, D. Bluestein, Platelet activation in a circulating flow loop: combined effects of shear stress and exposure time, Platelets 14 (3) (2003) 143–149.

[30] E. F. Grabowski, Platelet aggregation in flowing blood at a site of injury to an endothelial cell monolayer Blood 75 (2) (1990) 390–398.
URL http://www.ncbi.nlm.nih.gov/pubmed/2104767

[31] D. L. Bark, Jr, A. N. Para, D. N. Ku, Correlation of thrombosis growth rate to pathological wall shear rate during platelet accumulation, Biotechnology and bioengineeringdoi:10.1002/bit.24537.
URL http://www.ncbi.nlm.nih.gov/pubmed/22539078

[32] C. Karmonik, J. Bismuth, M. G. Davies, A. B. Lumsden, Computational fluid dynamics as a tool for visualizing hemodynamic flow patterns, Methodist DeBakey Cardiovascular Journal 5 (3) (2009) 26–33.
URL http://www.ncbi.nlm.nih.gov/pubmed/20308961

[33] G. Berti, @neurIST D23v2 - Analysis Protocols Version 2 (2010).
URL http://www.aneurist.org/UserFiles/File/PUBLIC_DELIVERABLES/D23v2_v1.2_final.pdf

[34] A. Chaniotis, L. Kaiktsis, D. Katritsis, E. Efstathopoulos, I. Pantos, V. Marmarellis, Computational study of pulsatile blood flow in prototype vessel geometries of coronary segments, Physica medica : PM : an international journal devoted to the applications of physics to medicine and biology : official journal of the Italian Association of Biomedical Physics (AIFB) 26 (3) (2010) 140–156. doi:10.1016/j.ejmp.2009.03.004.

[35] J. Y. Moon, D. C. Suh, Y. S. Lee, Y. W. Kim, J. S. Lee, Considerations of Blood Properties, Outlet Boundary Conditions and Energy Loss Approaches in Compu Neurointervention 9 (1) (2014) 1–8. doi:10.5469/neuroint.2014.9.1.1.
URL http://www.ncbi.nlm.nih.gov/pmc/articles/PMC3955817/

[36] E. Merrill, Rheology of Blood, Physiological Reviews 49 (4) (1969) 863–884.

[37] K. K. Yeleswarapu, M. V. Kameneva, K. R. Rajagopal, J. F. Antaki, The flow of blood in tubes: theory and experiment, Mechanics Research Communications 25 (3) (1998) 257–262. doi:10.1016/S0093-6413(98)00036-6.
URL http://www.sciencedirect.com/science/article/pii/S0093641398000366

[38] W.-T. Wu, F. Yang, J. F. Antaki, N. Aubry, M. Massoudi, Study of blood flow in several benchmark micro-channels using a two-fluid approach, International Journal of Engineering Science 95 (2015) 49–59. doi:10.1016/j.ijengsci.2015.06.004.
URL http://www.sciencedirect.com/science/article/pii/S0020722515000890

[39] P. D. Ballyk, D. A. Steinman, C. R. Ethier, Simulation of non-Newtonian blood flow in an end-to-side anastomosis, Biorheology 31 (5) (1994) 565–586.
URL http://www.ncbi.nlm.nih.gov/pubmed/7833458

[40] J. Boyd, J. M. Buick, S. Green, Analysis of the Casson and Carreau-Yasuda non-Newtonian blood models Physics of Fluids 19 (2007) 3103. doi:10.1063/1.2772250.
URL http://adsabs.harvard.edu/abs/2007PhFl...19i3103B

[41] J. Chen, X.-Y. Lu, Numerical investigation of the non-Newtonian pulsatile blood flow in a bifurcation mo Journal of biomechanics 39 (5) (2006) 818–832. doi:10.1016/j.jbiomech.2005.02.003.
URL http://www.ncbi.nlm.nih.gov/pubmed/16488221

[42] G. Pontrelli, Pulsatile blood flow in a pipe, Computers & Fluids 27 (3) (1998) 367–380. doi:10.1016/S0045-7930(97)00041-8.
URL http://www.sciencedirect.com/science/article/pii/S0045793097000418

[43] X. Y. Xu, M. W. Collins, A review of the numerical analysis of blood flow in arterial bifurcations, Proceedings of the Institution of Mechanical Engineers. Part H, Journal of Engineering in Medicine 204 (4) (1990) 205–216.
URL http://www.ncbi.nlm.nih.gov/pubmed/2090123

[44] F. M. White, Fluid Mechanics, 6th Edition, McGraw-Hill Higher Education, Pages 3-48, 2009.

[45] J. Al-Sukhun, H. Penttilä, N. Ashammakhi, Microvascular stress analysis: Part II. Effects of vascular wall compliance on blood flow at the graft/recipient vessel junction, The Journal of Craniofacial Surgery 22 (3) (2011) 883–887. doi:10.1097/SCS.0b013e31820f8004.

[46] Y. Huang, D. Tong, S. Zhu, L. Wu, Q. Mao, Z. Ibrahim, W. P. A. Lee, G. Brandacher, J. U. Kang, Evaluation of microvascular anastomosis using real-time, ultra-high-resolution, Fourier domain Doppler optical coherence tomography, Plastic and Reconstructive Surgery 135 (4) (2015) 711e–20e. doi:10.1097/PRS.0000000000001124.

[47] R. D. Acland, Practice Manual for Microvascular Surgery, 2nd Edition, Mosby, 1988.

[48] S. Shurey, C. Green, Basic Microsurgical Techniques: A Laboratory Manual, Surgical Research Department, NPIMR, Northwick Park Hospital, Middlesex, UK, 2011.

Microarterial anastomoses: a parameterised computational study examining the effect of suture position on intravascular blood flow

Highlights:

- Haemodynamics of microarterial anastomoses were modelled using Computational Fluid Dynamics (CFD)
- High Shear Strain Rates (SSR) are a known precipitant of platelet aggregation
- Greater suture angles from the standard perpendicular placement cause greater SSRs
- Sutures placed closely together cause greater SSRs
- Small variance in all parameters does not significantly influence flow properties